The Structural Basis for the Intrinsic Disorder of the Actin Filament: The "Lateral Slipping" Model

Andreas Bremer,* Robert C. Millonig,*‡ Rosmarie Sütterlin,* Andreas Engel,* Thomas D. Pollard,‡ and Ueli Aebi*‡

*M. E. Müller-Institute for High-Resolution Electron Microscopy at the Biocenter, University of Basel, CH-4056 Basel, Switzerland; and ‡Department of Cell Biology and Anatomy, The Johns Hopkins University School of Medicine, Baltimore, Maryland 21205

Abstract. Three-dimensional (3-D) helical reconstructions computed from electron micrographs of negatively stained dispersed F-actin filaments invariably revealed two uninterrupted columns of mass forming the "backbone" of the double-helical filament. The contact between neighboring subunits along the thus defined two long-pitch helical strands was spatially conserved and of high mass density, while the intersubunit contact between them was of lower mass density and varied among reconstructions. In contrast, phalloidin-stabilized F-actin filaments displayed higher and spatially more conserved mass density between the two long-pitch helical strands, suggesting that this bicyclic hepta-peptide toxin strengthens the intersubunit contact between the two strands. Consistent with this distinct intersubunit bonding pattern, the two long-pitch helical strands of unstabilized filaments were sometimes observed separated from each other over a distance of two to six subunits, suggesting that the intrastrand intersubunit contact is also physically stronger than the interstrand contact. The resolution of the filament reconstructions, extending to 2.5 nm axially and radially, enabled us to reproducibly "cut out" the F-actin subunit which measured 5.5 nm axially by 6.0 nm tangentially by 3.2 nm radially. The subunit is distinctly polar with a massive "base" pointing towards the "barbed" end of the filament, and a slender "tip" defining its "pointed" end (i.e., relative to the "arrowhead" pattern revealed after stoichiometric decoration of the filaments with myosin subfragment 1). Concavities running approximately parallel to the filament axis both on the inner and outer face of the subunit define a distinct cleft separating the subunit into two domains of similar size: an inner domain confined to radii ≤2.5-nm forms the uninterrupted backbone of the two long-pitch helical strands, and an outer domain placed at radii of 2–5-nm protrudes radially and thus predominantly contributes to the outer part of the massive base. Quantitative evaluation of successive crossover spacings along individual F-actin filaments revealed the deviations from the mean repeat to be compensatory, i.e., short crossovers frequently followed long ones and vice versa. The variable crossover spacings and diameter of the F-actin filament together with the local unraveling of the two long-pitch helical strands are explained in terms of varying amounts of compensatory "lateral slipping" of the two strands past each other roughly perpendicular to the filament axis. This intrinsic disorder of the actin filament may enable the actin moiety to play a more active role in actin-myosin–based force generation than merely act as a rigid passive cable as has hitherto been assumed.

ACTIN ranks among the most abundant and highly conserved eukaryotic proteins, and it serves vital functions in muscle contraction, cellular motility, intracellular transport, and in the regulation of the structure and dynamics of the cytoplasmic matrix. To ensure spatial and temporal control over these diverse functions, actin interacts with itself, with a myriad of actin-binding and regulatory proteins, as well as with small effector molecules (for recent reviews see Pollard, 1990; Vandekerckhove, 1990).

Isolated as a 42-kD monomer (i.e., G-actin), actin can be polymerized in vitro into filaments (i.e., F-actin) which in muscle cells, together with tropomyosin and troponin, form the thin filaments. By EM, Huxley (1963) and Hanson and Lowy (1963) have uncovered F-actin as a double-helical filament consisting of two intertwined "long-pitch" helical strands of roughly spherical actin subunits. With 13 subunits per right-handed long-pitch helical turn, the axial subunit repeat of 5.5 nm amounts to a pitch of 71.5 nm. The two long-pitch helical strands are axially staggered by half the axial subunit spacing (i.e., 2.75 nm) and thus cross each other every 35.75 nm. An alternative geometrical description of the F-actin filament structure is that of a 5.9-nm pitch one-start

"genetic" helix with 13 subunits per 6 left-handed turns (for reviews see Aebi et al., 1986; Holmes and Kabsch, 1991).

The first three-dimensional (3-D) reconstruction of a negatively stained dispersed thin filament as well as of F-actin filaments masked out from paracrystalline arrays revealed slightly elongated subunits with strong intersubunit contacts along the two long-pitch helical strands but only tenuous contacts between the two strands (Moore et al., 1970). Subsequently, various qualitatively similar 3-D reconstructions primarily differing in the relative strength of the two types of intersubunit contacts (i.e., along and between the two long-pitch helical strands) were computed from F-actin or thin filaments masked out from paracrystalline arrays (reviewed by Amos, 1985; Egelman, 1985). Such paracrystalline arrays provided straight and highly ordered filament stretches, but it could not be excluded that interdigitation and/or superposition of adjacent filaments introduced artifacts into the reconstruction (see Smith et al., 1983; Aebi et al., 1986). Surprisingly however, 3-D reconstructions of frozen-hydrated dispersed F-actin filaments also differed in the relative strength of the intersubunit contacts: while the reconstruction of Trinick et al. (1986) revealed genetic helix contact only, the recent reconstruction of Milligan et al. (1990) shows significant long-pitch helix contact and thus appears remarkably similar to reconstructions of negatively stained dispersed F-actin filaments published earlier (Aebi et al., 1986). As pointed out by Milligan et al. (1990), a high resolution structure of F-actin filaments based on electron microscope images "provides an important framework for constructing an atomic model of F-actin from the high-resolution X-ray structure of the actin monomer."

Seymour and O'Brien (1980) first attempted to localize tropomyosin in negatively stained thin filaments. Next, O'Brien et al. (1983) reconstructed thin filaments masked out from negatively stained single-layered paracrystals and resolved a distinct ∼2.0-nm diameter mass contribution at a filament radius of 4 nm. This mass was interpreted as tropomyosin and lined the cleft between the inner and outer domain of the subunits along the two long-pitch helical strands on the outside of the filament. This result has later been confirmed with frozen-hydrated specimens (Milligan and Flicker, 1987; Milligan et al., 1990).

The 3-D structure of the actin molecule was determined by EM of 2-D crystalline actin sheets (Aebi et al., 1981; Smith et al., 1983, 1984), and by X-ray diffraction of 3-D actin-DNase I (Sakabe et al., 1983; Kabsch et al., 1985) and actin-profilin co-crystals (Schutt et al., 1989). Accordingly, the subunit invariably appeared bilobed, composed of a larger and a smaller domain. Eventually, the atomic structure of the actin-DNase I complex (Kabsch et al., 1990) has confirmed that the actin molecule consists of two domains of similar size (i.e., differing by ∼5% in mass) separated by a distinct cleft accommodating the nucleotide (i.e., ATP or ADP) and the high-affinity binding site for a divalent cation, for G-actin believed to be Mg^{2+} under physiological conditions. Despite little detectable sequence homology, there is a striking structural similarity of actin with hexokinase and the NH_2-terminal 44-kD ATPase fragment of the heat-shock cognate 70 (HSC-70) (Holmes and Kabsch, 1991; Flaherty et al., 1991).

Molecular modeling of the F-actin filament structure has been pursued for several years. In a first attempt, the actin subunit was approximated by two interpenetrating 3.8-nm diameter spheres with a center-to-center separation of 3.0 nm revealing a 9.5-nm diameter filament with intersubunit contacts along the genetic helix only (Egelman and DeRosier, 1983). Next, Aebi and co-workers (Smith et al., 1983, 1984; Aebi et al., 1986) aligned the 1.5-nm resolution actin sheet subunit (Smith et al., 1983) within F-actin filament 3-D reconstructions and revealed an 8.5-nm diameter filament with predominant long-pitch helix contact. Most recently, by fitting the atomic structure of the actin molecule (Kabsch et al., 1990) to ≤1.0-nm resolution F-actin fiber diffraction data, Holmes et al. (1990) arrived at a 9.0–9.5-nm maximum diameter atomic model of the F-actin filament. The extensive long-pitch and more tenuous genetic helix intersubunit contacts observed with this atomic model are in excellent qualitative agreement with the 3-D reconstructions of Aebi et al. (1986) and Milligan et al. (1990). It is conceivable that the structure of the actin molecule in the actin-DNase I complex differs slightly from that of G-actin (Holmes and Kabsch, 1991). In addition, polymerization of G-actin into F-actin is accompanied by sequential conformational changes (reviewed in Pollard, 1990). Therefore, the F-actin filament structure can only be modeled, rather than exactly solved, using the atomic structure of the actin moiety of actin-DNase I co-crystals and F-actin fiber diffraction data.

Variable crossover spacings in negatively stained (Hanson, 1967) and frozen-hydrated (Trinick et al., 1986) preparations as well as the variable filament width (reviewed in Aebi et al., 1986; see, e.g., Fig. 7 b of Bullard et al., 1985) indicate that F-actin filaments may locally significantly deviate from perfect helical symmetry (reviewed by Holmes and Kabsch, 1991). Comparing negatively stained and frozen-hydrated F-actin filaments suggested intrinsic filament disorder, rather than preparation artifacts, to give rise to these structural variations (Stokes and DeRosier, 1987). Egelman et al. (1982) have attempted to model and quantitate the variable crossover spacings as cumulative angular disorder due to a random variable twist of the subunits along the genetic helix. As attractive their model may be, it is difficult to reconcile within the constraints of (a) the known precision of protein-protein interactions (reviewed in Erickson, 1989) and (b) the atomic model of the actin filament (Holmes and Kabsch, 1991) and, thus, may have to be reevaluated.

Here we report 3-D reconstructions of negatively stained dispersed F-actin filaments and of F-actin filaments which have been stabilized with phalloidin, a bicyclic heptapeptide, one of the toxins of the toadstool *Amanita phalloides* (Faulstich et al., 1977; reviewed in Cooper, 1987). Using S1-decorated F-actin seeds, we have determined the orientation of the F-actin subunit relative to the "barbed" and the "pointed" ends of the F-actin filament. We have quantitatively evaluated successive crossover spacings along individual F-actin filaments as well as the crossover spacing frequency distributions of negatively stained F-actin filaments polymerized in the absence and presence of phalloidin, and explored conditions where "local unraveling" of the two long-pitch helical strands is observed. Based on our structural data and incorporating a number of published results, we propose compensatory "lateral slipping" of the two long-pitch helical strands relative to each other—rather than cumulative angular disor-

der of the subunits along the genetic helix (Egelman et al., 1982)—to be the structural basis of the intrinsic disorder of F-actin that gives rise to variable crossover spacings and filament diameters.

Materials and Methods

Materials

Unless specified otherwise, all chemicals were of analytical or best available grade. ATP (A-2383, sodium salt, grade I) and phalloidin from *Amanita phalloides* (P-2141) were purchased from Sigma Chemical Co. (St. Louis, MO). Electron image film SO-163 and developer D-19 were products of Eastman Kodak Co. (Rochester, NY). Uranyl formate was obtained from BDH Chemicals Ltd. (Poole, England), and phosphotungstic acid was purchased from Fluka Chemie AG (Buchs, Switzerland). Glutaraldehyde was a product of Electron Microscopy Sciences (Ft. Washington, PA). For all experiments, water deionized by a Skan NANOpure cartridge system (Skan AG, Basel-Allschwil, Switzerland) with a specific residual resistivity of better than 18 MΩcm was used.

Preparation of G-Actin

Rabbit skeletal muscle actin was isolated and purified according to Millonig et al. (1988), the resulting G-actin peak fractions stored at 4°C in 2.5 mM imidazole, pH 7.4, 0.2 mM $CaCl_2$, 0.2 mM ATP, 0.005% NaN_3 (buffer A) and used within 2–4 wk.

Preparation of F-Actin Filaments

Aliquots of G-actin, typically at a protein concentration of 1 mg/ml, were dialyzed overnight at 4°C into freshly prepared buffer A, polymerized by adding $MgCl_2$ to 2 mM and/or KCl to 50 mM, and incubated at room temperature for at least 2 h. The F-actin filaments were pelleted by centrifugation for 10 to 15 min at 150,000 g and resuspended in the original volume of polymerization buffer. Phalloidin-stabilized F-actin filaments were polymerized in a twofold molar excess of phalloidin relative to actin. Preparation and elongation of glutaraldehyde-fixed, S1-decorated F-actin filament seeds was performed as previously described (Cooper and Pollard, 1982) except for polymerizing the actin in buffer A containing 1 mM $MgSO_4$ and 50 mM KCl.

Specimen Preparation and EM

F-actin filaments were diluted with polymerization buffer in a test tube to a final concentration of ∼0.2 mg/ml and instantly applied to a lightly glow-discharged (Aebi and Pollard, 1987) EM grid which had been washed with a drop of polymerization buffer immediately before use (Millonig et al., 1988). Alternatively, F-actin filaments were diluted by "injecting" a 1-μl aliquot of F-actin into a 5-μl drop of polymerization buffer deposited on the grid (Aebi et al., 1986). Sample adsorption, washing, and negative staining with 0.75% uranyl formate, pH 4.25, were performed as described (Millonig et al., 1988). For negative staining with 2% Na-phosphotungstate, pH 7.0, we followed essentially the same protocol. EM was performed using a Hitachi H-7000 electron microscope (Hitachi Ltd., Tokyo, Japan) operated at an accelerating voltage of 100 kV. Micrographs were recorded under low-dose conditions at 50,000 × nominal magnification on Kodak SO-163 electron image film which was developed for 6 min at room temperature in Kodak D-19 developer diluted threefold with water. The effective magnification of the microscope was calibrated using negatively stained catalase crystals as a standard (Wrigley, 1968).

Digital Image Processing

Micrographs were screened for well preserved and uniformly stained, relatively straight filament stretches with evenly spaced crossovers. Such filament stretches of typically five to ten crossovers in length were scanned on an Eikonix 850 8-bit CCD imaging camera (Eikonix, Bedford, MA). Slightly curved filament stretches were next digitally unbent using a routine implemented in the SEMPER image processing package (Saxton et al., 1979) run on an Apollo graphics workstation (Apollo Computer Inc., Chelmsford, MA). To achieve this, we defined the filament axis by fitting a cubic spline (Dierckx, 1980) through peaks in the cross-correlation of the filament with a reference crossover repeat or, alternatively, through points

defined interactively. The image of the unbent filament stretch was computed by bilinearly interpolating pixel values along equidistant normals to the curvilinear coordinate system defined by the spline (see also Steven et al., 1985; Egelman, 1986). All subsequent steps of digital image processing were performed using the modular program package MDPP (Smith, 1978) run on a DEC VAX 8200 computer (Digital Equipment Corp., Maynard, MA). First, the optimal mean helical repeat was determined individually for each filament stretch (typically over two to six crossovers) by systematically varying it to minimize the power loss upon longitudinal averaging over the number of helical repeats within this stretch. Next, a filament stretch containing an integer number of optimized helical repeats was D(Z,k)-filtered (Smith and Aebi, 1974) using the integer helical selection rule giving the smallest power loss. The selection rules tried included (−6/13) (i.e., $l = -6n + 13m$), (−12/27), (−13/27), (−13/28), (−18/40), (−19/40), and (−19/41). In this step, minimizing the power loss was also used as a criterion to refine the radial position of the helix axis.

3-D Helical Reconstructions

D(Z,k)-filtered helical repeats were Fourier transformed and the layer lines contributing intensities significantly above the background (i.e., the equator, 1st, 2nd, 5th, 6th, 7th, 8th, and 13th layerline in the case of $l = -6n + 13m$) were extracted. These layer line data were used to compute 3-D reconstructions by a Fourier-Bessel transformation method (see DeRosier and Moore, 1970; Smith et al., 1976, 1983). For model building, a hydrated protein mass density of 810 D/nm^3 (see Taylor and Amos, 1981; Smith et al., 1983) was assumed. Either 10 consecutive 0.275-nm-spaced sections normal to the filament axis were contoured to include 100% mass of the 42-kD actin subunit, or alternatively, volume rendering of stacks of 0.275-nm-spaced sections was performed computationally using the "marching cube" algorithm GRAPHCUBE (Lorensen and Cline, 1987) implemented by Ed Combs on an Apollo graphics workstation (Apollo Computer Inc., Chelmsford, MA) in our laboratory.

Determination of Crossover Spacings

Digitized F-actin filament stretches, typically 10 to 12 crossovers long, were computationally unbent as described above. The resulting images were filtered in Fourier space by masking out the spatial frequencies ⩾(30.0 nm)$^{-1}$ and those ⩽(250.0 nm)$^{-1}$. Thus, filtered images were projected perpendicular to the filament axis, a procedure that revealed crossover points as local maxima. Finally, the coordinates of these maxima were determined by a computational peak search and used to compute successive crossover spacings along individual F-actin filaments.

Results

Specimen Preparation, EM, and Processing of the F-Actin Filament Data

As illustrated in Fig. 1 *a*, our improved protocol to prepare negatively stained, dispersed F-actin filaments (Aebi et al., 1986; Millonig et al., 1988) yielded significant numbers of well preserved and relatively straight filament stretches suitable for 3-D helical reconstruction. For comparison, Fig. 1 *b* shows F-actin filaments that have been polymerized in the presence of a 2:1 molar excess of the mushroom toxin phalloidin relative to actin (see below).

From such micrographs well preserved and uniformly stained filament stretches with evenly spaced crossovers were selected for 3-D helical reconstruction. Since most of the filament stretches that fulfilled all the above criteria were slightly bent, they were routinely unbent computationally (see Materials and Methods). The procedure is documented in Fig. 2 (*a–e*): *a* displays a digitized curved F-actin filament; *b*, its cross-correlation with a reference crossover repeat; *c*, peaks in the cross-correlation chosen to define the filament axis; *d*, the original filament with its axis defined by a cubic spline fitted through the peaks in *c* superimposed; and *e*, the resulting unbent filament. *f* displays a representative com-
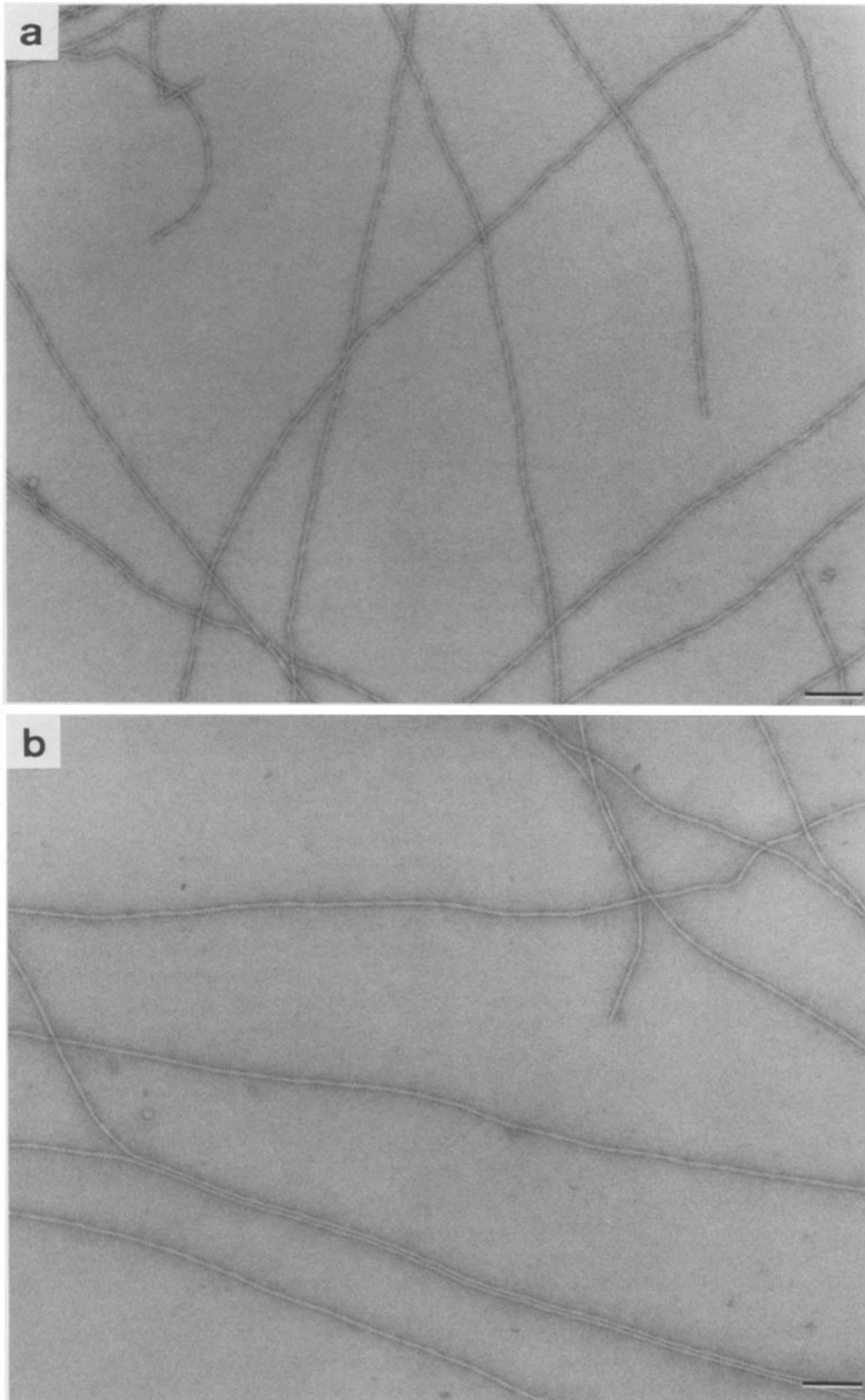
Figure 1. Electron micrographs of synthetic F-actin filaments negatively stained with 0.75 % uranyl formate, pH 4.25. Rabbit skeletal muscle G-actin was polymerized (*a*) with 2 mM MgCl₂/50 mM KCl and (*b*) with the same salts but in the presence of a 2:1 molar ratio of phalloidin to actin (see Materials and Methods). Bars: (*a* and *b*) 100 nm.

puted diffraction pattern of an unbent 10-crossover-repeat long filament stretch, i.e., ∿360 nm long. Particularly evident are the first and the sixth layerline that, in this example, contribute about equally to the total power. Comparisons of

3-D reconstructions obtained from straightened F-actin filaments with those obtained from initially straight F-actin filaments did not reveal any systematic differences (data not shown; see also Steven et al., 1985; Egelman, 1986).
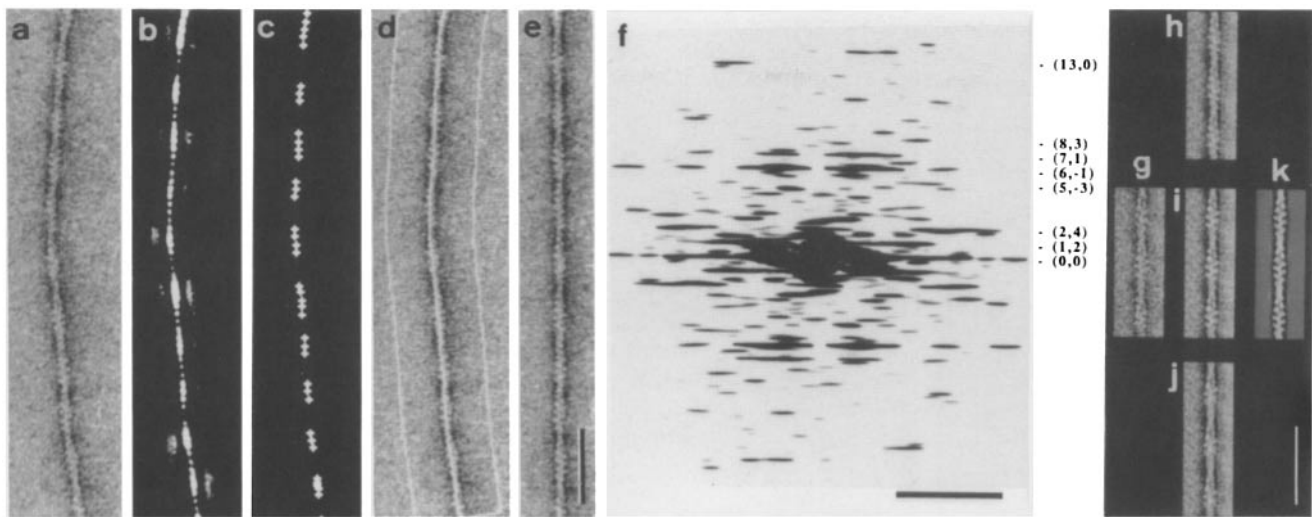
Figure 2. Digital processing of electron micrographs of negatively stained synthetic F-actin filaments as shown in Fig. 1. Actin filament preparation was as described in Materials and Methods, polymerizing the actin with 2 mM $MgCl_2$/50 mM KCl, and using 0.75% uranyl formate, pH 4.25, as the negative stain. A digitized, 10-crossover long actin filament stretch (*a*) and its cross-correlation with a reference crossover repeat (*b*). After a peak search (*c*), a cubic spline was fitted through selected peaks to define the filament axis (*d*). Image of the unbent filament stretch (*e*), computed by bilinear interpolation of pixel values along equidistant normals to the filament axis as defined by the spline. A representative computed diffraction pattern of a straightened 10-crossover long filament stretch with the (*l*, *n*) numbers marking the layer lines used for 3-D helical reconstruction is shown in *f*. An unbent 3-crossover long filament stretch (*g*) was longitudinally averaged over its optimized helical repeat (*i*) determined as described in Materials and Methods. To demonstrate the importance of optimizing the helical repeat, the same filament stretch was also longitudinally averaged assuming a two sample-point (i.e., 1.1 nm) longer (*h*), or a two sample–point shorter (*j*) helical repeat. The optimized and longitudinally averaged helical repeat shown in *i* was next D(Z,k)-filtered (*k*) as described in Materials and Methods, imposing the integer helical selection rule $l = -6n + 13m$. Bars: (*a–e*, *g–k*) 50 nm; (*f*) $(5 \text{ nm})^{-1}$

For each filament stretch, the helical repeat corresponding to its closest integer helical selection rule (see Materials and Methods) was optimized by systematically varying it to minimize the power loss upon longitudinal averaging. This approach allowed the average helical repeat of individual filament stretches to be determined to within one 0.55-nm sample point. The importance of this step to preserve structural information is illustrated in Fig. 2 (*g–j*), where an unbent three-crossover long filament stretch (*g*) has been averaged over its optimized helical repeat (*i*) versus a two sample–point longer (*h*) or a two sample–point shorter (*j*) repeat. Most of the filament stretches chosen for 3-D helical reconstruction were closest to the integer helical selection rule $l = -6n + 13m$ (see also DeRosier and Censullo, 1981; Aebi et al., 1986), i.e., (−6/13), with a few being closer to either (−13/28) or (−19/41). Next, as illustrated in Fig. 2 *k*, a filament stretch containing an integer number of optimized helical repeats (Fig. 2 *i*) was D(Z,k)-filtered (see Smith and Aebi, 1974). On average, 72.5 ± 7.1% (mean ± SD) of the total power was recovered after this filtering step, during which the radial position of the helix axis was also varied such as to minimize the power loss. This refinement step is important as a lateral displacement of the helix axis by one 0.55-nm sample point may significantly affect the quality of the reconstruction (data not shown).

3-D Helical Reconstruction of Dispersed F-Actin Filaments

D(Z,k)-filtered helical repeats (Fig. 2 *k*) were next Fourier transformed and the phase correlation between the two halves of the transform was monitored. Accordingly, for filament stretches with (−6/13) helical symmetry, the 1st, 2nd, 5th, 6th, 7th, 8th, and 13th layerlines contained helical information significantly above the background (see also Fig. 2 *f*). Therefore, these layerlines were extracted and together with the equator used to compute 3-D helical reconstructions as described in Materials and Methods. A global amplitude-weighted phase residual (parameter Q of DeRosier and Moore, 1970) was calculated for each F-actin filament reconstruction and ranged between 15° and 25° after refining the phase origin. The resolution of our datasets used for 3-D helical reconstruction typically extended to 2.5 nm both axially and radially.

Fig. 3 *a* is the sum of two similar reconstructions, both computed from three helical repeats, while Fig. 3 *b* is the sum of four similar reconstructions, all computed from four helical repeats. Contoured to include 100% mass, all our reconstructions reveal a pronounced intertwined, two-stranded structure (Fig. 3, *a* and *b*). Due to the distinct axial and radial mass density modulation, the individual actin subunits comprising the two long-pitch helical strands can readily be distinguished. Owing to the flatness of the actin subunit perpendicular to the filament axis (see also Figs. 4 and 5), in projection, the filaments appear narrowest where the two long-pitch helical strands lie side-by-side (average width 6.5 nm), and wider where they come to lie on top of each other (average width 7.5 nm). The maximum diameter as measured on end-on views (Fig. 3, *a* and *b*, *bottom panels*) ranged between 8 and 9 nm, for example 8.9 nm for the summed filament in *a* and 8.3 nm for that in *b*.

In more than 50 3-D helical reconstructions the inter-subunit contact along the two long-pitch helical strands was conserved, but the spatial extent and mass density of the con-
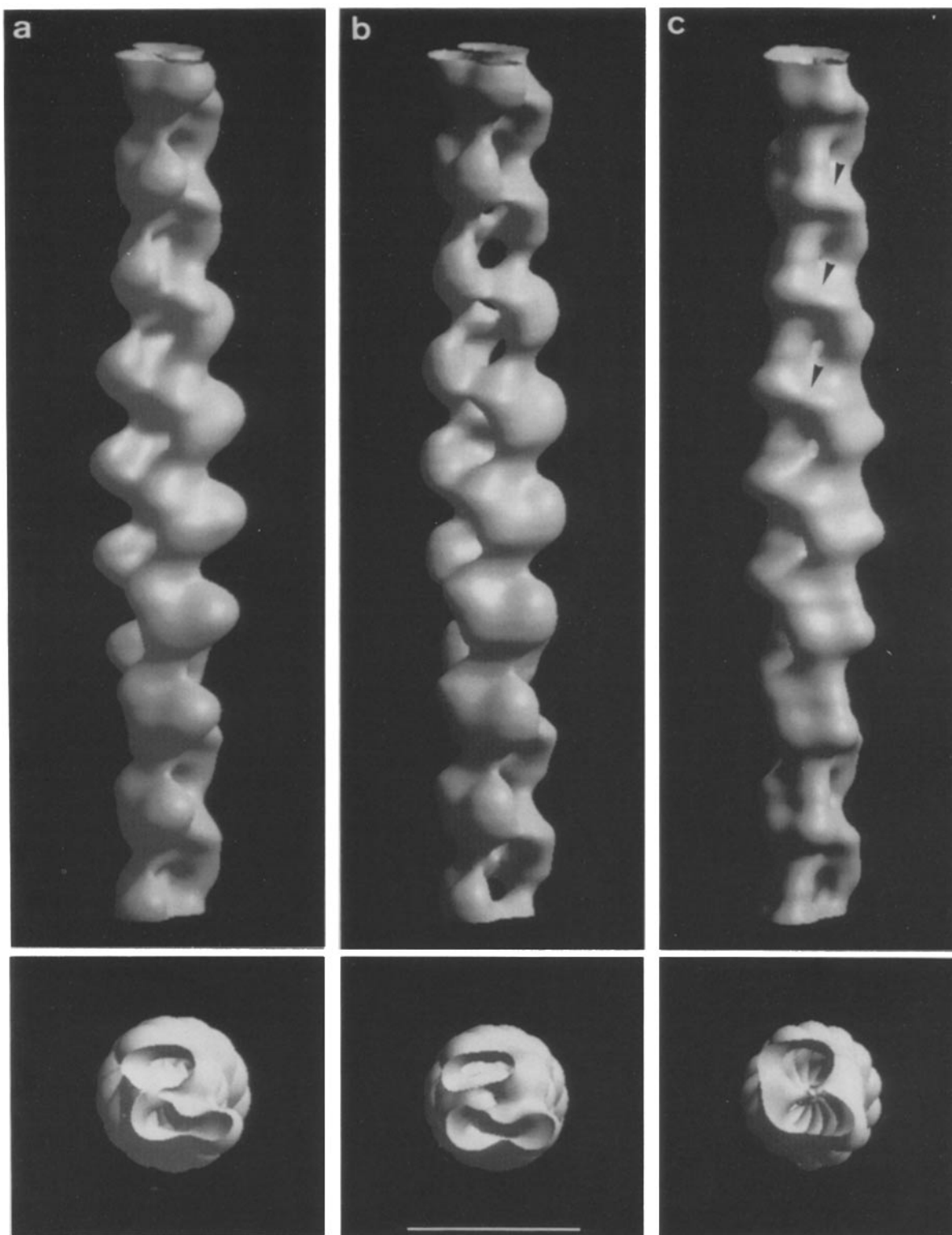
Figure 3. 3-D helical reconstructions of negatively stained actin filaments as shown in Fig. 1. (*a*) Sum of two similar reconstructions computed from two three-helical-repeat long stretches of unstabilized actin filaments (i.e., the filaments were polymerized as in Fig. 1*a*) with relatively strong contact between the two long-pitch helical strands, and (*b*) sum of four similar reconstructions computed from four 4-helical-repeat long unstabilized filament stretches with relatively weak contact between the two long-pitch helical strands. (*c*) Sum of three reconstructions computed from three four-helical-repeat long phalloidin-stabilized filament stretches (i.e., the filaments were polymerized as in Fig. 1 *b*). The lower panels of *a–c* display end-on views of the corresponding reconstructions shown in the upper panels. Using a "marching cube" algorithm (see Materials and Methods), all reconstructions have been volume rendered to include 100% mass assuming a hydrated mass density of 810 D/nm³. Bar, 10 nm.
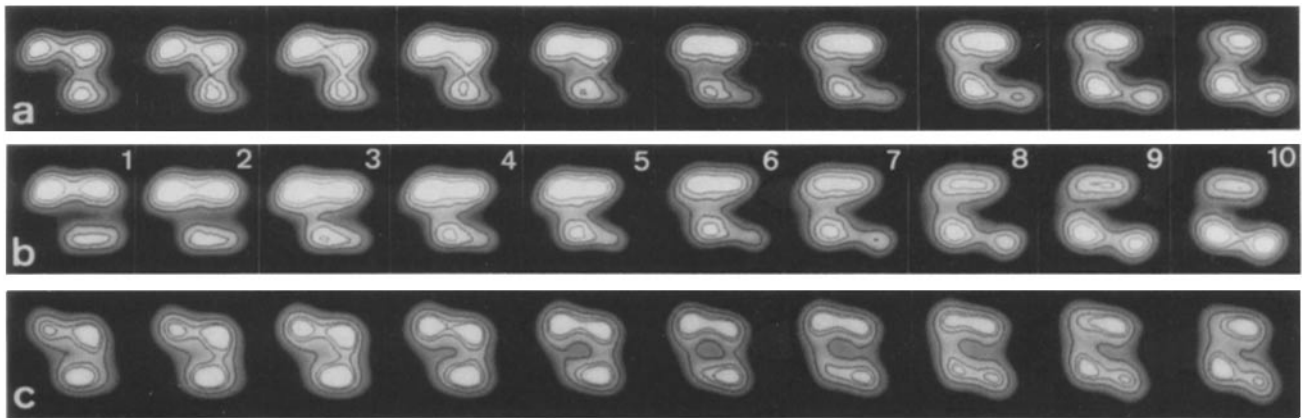
Figure 4. Stacks of ten 0.275-nm spaced sections normal to the filament axis defining exactly one actin subunit (i.e., each of the two long-pitch helical strands contributes one complementary half of a subunit) corresponding to the three reconstructions shown in Fig. 3. Superimposed onto the grey level representation of the sections are contours to include 100, 75, and 50%, respectively, of the total mass assuming a hydrated mass density of 810 D/nm^3. Lettering (*a–c*) is as in Fig. 3.

tact between these strands, as well as their relative radial displacement were variable. In this regard, the summed reconstructions shown in Fig. 3 (*a* and *b*) are averages of two distinct classes: the reconstruction shown in Fig. 3 *a* is representative for those having maximum, while that shown in Fig. 3 *b* is representative for those having minimum intersubunit contact between the two long-pitch helical strands. This difference is visualized more clearly in Fig. 4 (*a* and *b*), where the two summed reconstructions are displayed as stacks of ten 0.275-nm spaced sections normal to the filament axis with superimposed contours drawn to include 100, 75, and 50% of the total mass. To facilitate comparison, the two stacks of sections are aligned angularly and axially relative to each other. With the 8.9-nm diameter F-actin filament shown in Fig. 4 *a*, the contact between the two long-pitch helical strands extends over all 10 sections, and is of relatively high mass density with some contact persisting at the 75% mass level (i.e., sections 2, 3, and 4). As a comparison, the 8.3-nm diameter reconstruction depicted in Fig. 4 *b* reveals spatially less extended contact between the two strands, i.e., sections 1, 2, 9, and 10 exhibit no contact, and in sections 3 to 8 the contacts are broken at a mass contouring level of ≤75%. In contrast, the uninterrupted intersubunit contact along the two long-pitch helical strands is invariably of high mass density (i.e., it persists even at a contouring level to include only 50% mass), and spatially, it is confined to relatively low filament radii (≤2.5 nm). Taken together, in all our reconstructions the genetic helix intersubunit contact, i.e., that between the two long-pitch helical strands, was always of lower mass density and spatially more variable than the long-pitch helix intersubunit contact.

Obtaining an F-Actin Subunit Model

The two long-pitch helical strands are axially staggered by 2.75 nm (i.e., half the axial subunit repeat) relative to each other (Huxley, 1963; Hanson and Lowy, 1963). Thus, the ten 0.275-nm spaced sections each shown in Fig. 4 (*a* and *b*) define exactly one subunit, i.e., each of the two strands contributes one complementary half of a subunit. Therefore, an F-actin subunit model can be obtained from such a stack of

sections by drawing a "smooth cut" between the two strands, i.e., following the density minima separating the contributions from the two strands present in each section (for details, see Aebi et al., 1986). In contrast, due to the uninterrupted mass density along the two long-pitch helical strands, separating adjacent subunits within a strand was more ambiguous. Nevertheless, the distinct radial modulation of the two strands (see Fig. 3) prompted us to define the section that revealed the minimum spatial extent as the "top" of the subunit. Accordingly, in each stack of Fig. 4, the lower half of section 1 defines the top of the subunit, while the upper half of section 10 defines its bottom. In Fig. 5 (*a* and *b*), different views of the resulting 20-section F-actin subunit models obtained from the two summed filament reconstructions in Fig. 3 (*a* and *b*) are presented. Both subunits are elongated perpendicular to the filament axis and consist of a massive "base" and a slender "tip", rendering them distinctly polar in the axial direction. As highlighted in Fig. 5 *d* for the subunit shown in Fig. 5 *b*, a distinct, slightly curved concavity runs approximately parallel to the filament axis both on the outer (*left*) and the inner (*right*) face of the subunit. These two concavities define a cleft that separates the subunit into two domains of similar size: the inner domain (I), confined to low filament radii (i.e., ≤2.5 nm), forms the backbone of the two long-pitch helical strands and is implicated in both the long-pitch as well as the genetic helix intersubunit contact; and the outer domain (O), confined to high filament radii (i.e., 2–5 nm), at its bottom forms part of the contact between the two long-pitch helical strands. The overall dimensions of the subunits obtained from unstabilized F-actin filaments (Fig. 5, *a*, *b*, and *d*) are 5.5 nm axially by ∼6.0 nm tangentially by ∼3.2 nm radially.

Structural Analysis of Phalloidin-stabilized F-Actin Filaments

A summed, 8.1-nm diameter reconstruction of three four-helical-repeat long phalloidin-stabilized F-actin filament stretches is displayed in Fig. 3 *c*. Here, a massive "bridge" (see *arrowheads*) is formed between the middle part of the inner domain of a subunit within one long-pitch helical strand and the contact region (i.e., top and bottom) of two
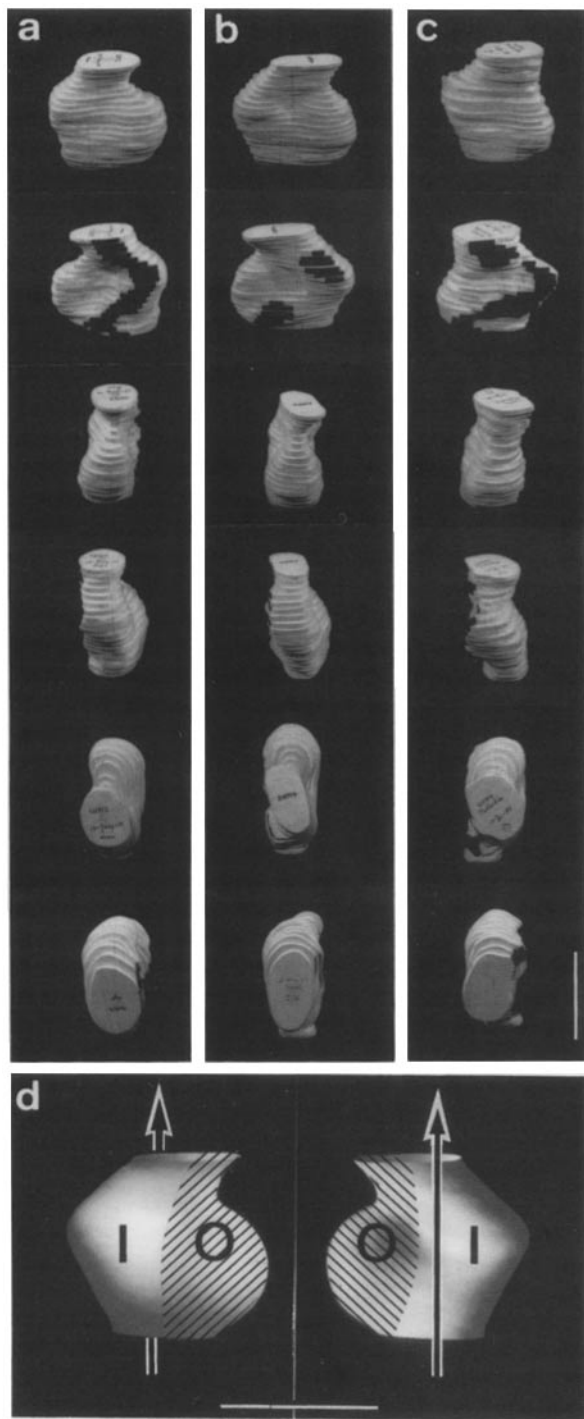
Figure 5. Different views of individual F-actin subunits "cut out" from the 3-D helical reconstructions shown in Fig. 3 as described in Results. Lettering a, b, c is as in Figs. 3 and 4. The subunits are contoured to include 100% of the total mass assuming a hydrated mass density of 810 D/nm³. The intersubunit contact areas between the two long-pitch helical strands have been shaded in dark. (d) Blow-up views of the subunit depicted in b with the filament axis superimposed. Concavities running approximately parallel to the filament axis both on the outer (*left view*) and inner (*right view*) face of the subunit define a distinct cleft separating the subunit into the inner domain (I; *white*) confined to ≤2.5-nm radii, and an outer domain (O; *hatched*) placed at 2-5-nm radii. Bars: (a-d) 5 nm.
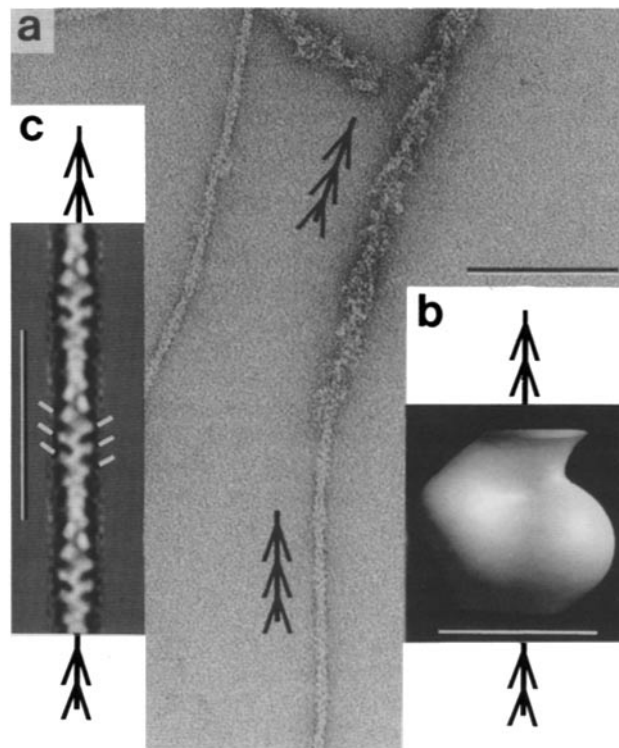

Figure 6. Polarity of the F-actin subunit (b) and the F-actin filament (c), respectively, relative to the "barbed" and "pointed" ends of the actin filament as defined by the "arrowhead" pattern (a) obtained upon stoichiometric decoration of the filament with myosin S1. (a) Partially S1-decorated "hybrid" F-actin filaments obtained by elongating S1-decorated, glutaraldehyde-fixed filament seeds with actin. The S1-defined polarity is marked schematically by stretches of arrowheads. (b) The slender "tip" of the subunit is oriented towards the pointed end, while its massive "base" faces the barbed end. (c) Helically filtered F-actin filament image revealing an intrinsic "mini-arrowhead" pattern that is of opposite polarity compared to the S1-decoration pattern. Bars: (a) 100 nm; (b) 5 nm; and (c) 50 nm.

adjacent subunits belonging to the other long-pitch helical strand (see also Fig. 5 c). This bridge appears to mediate a "mutual embracing" of the two long-pitch helical strands, thus resulting in a more compact packing of the two long-pitch helical strands relative to each other. In contrast to unstabilized F-actin filaments, the contact between the two long-pitch helical strands is reasonably conserved among phalloidin-stabilized F-actin filaments. In fact, as documented in Fig. 4 c, it resembles the genetic helix contact of the 8.9-nm diameter summed reconstruction presented in Figs. 3 a and 4 a, with some contact (i.e., sections 2 and 3) persisting at the 75% mass level.

The subunit deduced from phalloidin-stabilized F-actin filaments is distinct from those of unstabilized F-actin (Fig. 5, compare c with a and b). The overall dimensions are 5.5 × 5.8 × 3.3 nm. The outer domain of the phalloidin-stabilized F-actin subunit appears to be partially "pushed" into the inner domain (compare first two subunit views in Fig. 5, a-c). While the radially outermost part of the inner domain is angularly bent inwards, the radially outermost part of the outer domain appears being bent outwards (Fig. 4 c). The dark-shaded areas on the subunits in Fig. 5 highlight the con-
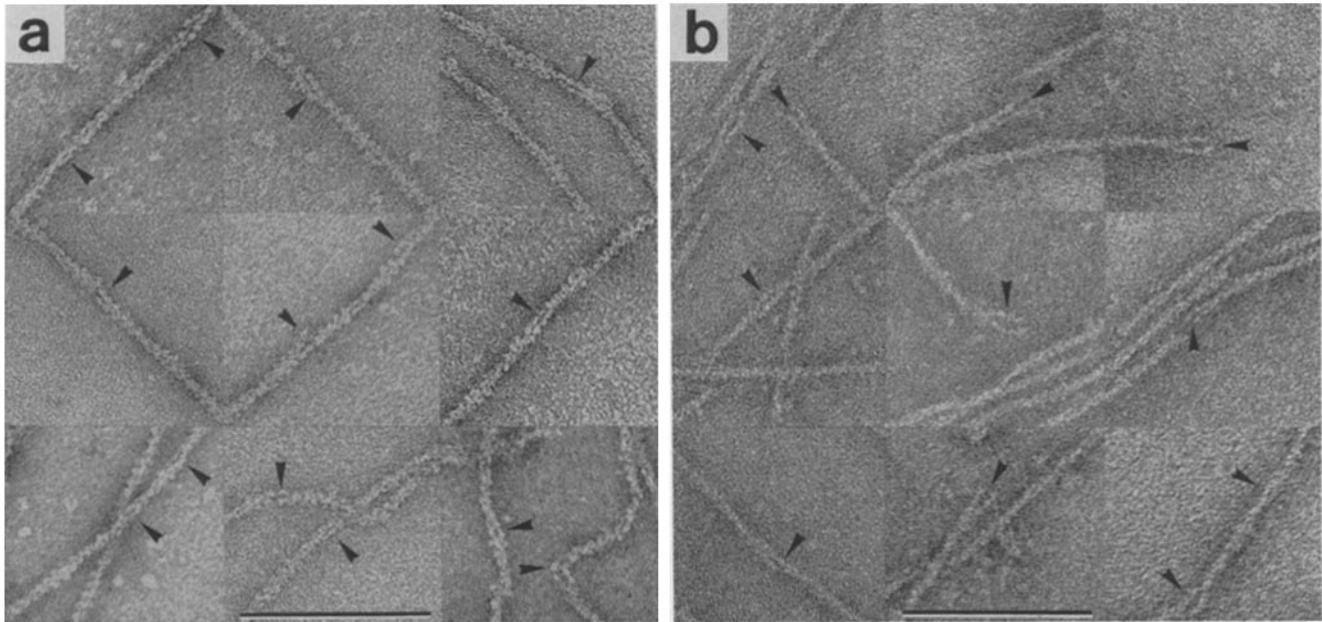
Figure 7. Examples of F-actin filament stretches that are locally unraveled into their two long-pitch helical strands. Actin filaments were polymerized with 2 mM MgCl₂/50 mM KCl and negatively stained with either 0.75% uranyl formate, pH 4.75 (*a*), or 2% sodium phosphotungstate, pH 7.0 (*b*). Arrowheads point to short "loops" or "splayed ends." Bars: (*a* and *b*) 100 nm.

tact areas between the two long-pitch helical strands, i.e., the density minimum separating the mass contributions from the two strands (see above). The contact between the two long-pitch helical strands of the 8.9-nm diameter unstabilized (Fig. 5 *a*) and the 8.1-nm diameter phalloidin-stabilized (Fig. 5 *c*) reconstructions are quite similar: they follow an uninterrupted, almost sinusoidal path along the inner domain close to the filament axis. The altered shape of the phalloidin-stabilized F-actin subunit gives rise to a higher mass density and more kinked intersubunit contact interface, and thus allows for a closer proximity of the two long-pitch helical strands (Figs. 4 *c* and 5 *c*). In contrast, the subunit deduced from the 8.3-nm diameter reconstruction (Fig. 3 *b*) reveals two spatially separated contact areas (Fig. 5 *b*), indicating a less extensive intersubunit contact along the genetic helix.

Identification of the "Barbed" and "Pointed" Ends of the F-Actin Filament Reconstructions

3-D reconstruction of F-actin filament stretches elongated from S1-decorated filament seeds (Fig. 6 *a*) enabled us to orient our F-actin filament reconstructions (Fig. 3), and hence F-actin subunit models (Fig. 5) relative to the "barbed" and "pointed" ends of the F-actin filament. As illustrated in Fig. 6 *b*, the slender tip of the F-actin subunit is oriented towards the pointed end, and the massive base towards the barbed end of the S1-decorated F-actin filament. Helically filtered filament images also display a distinct polarity (Fig. 6 *c*): accordingly, the "mini-arrowhead" pattern of undecorated filaments points in the opposite direction of the "arrowhead" pattern defined by S1-decoration and therefore is of opposite polarity (see also Vibert and Craig, 1982; O'Brien et al., 1983).

Local Unraveling of F-Actin Filaments into Their Two Long-pitch Helical Strands

According to all our 3-D helical reconstructions of unstabi-

lized F-actin filaments (Figs. 3, *a* and *b* and 4, *a* and *b*), the higher mass density intersubunit contact was invariably along, and not between, the two long-pitch helical strands. However, in the case of negatively stained specimens, the mass density of an intersubunit contact does not necessarily reflect its physical strength. Therefore, if correct, this intersubunit bonding pattern should allow the F-actin filament to behave as two independent long-pitch helical strands that may "laterally slip" past each other in an approximately radial direction. Such movements, if resulting in complete strand separation, cause "local unraveling", i.e., extending over a few subunits, of the two long-pitch helical strands into "loops" and/or "splayed ends." As documented in Fig. 7 *a*, such locally unraveled F-actin filament stretches could indeed be found in our preparations of unstabilized F-actin filaments when negatively stained with uranyl formate. With Na-phosphotungstate as the negative stain, even more dramatic examples of looping and particularly splaying were observed (Fig. 7 *b*). In agreement with the higher mass density intersubunit contact along the two long-pitch helical strands (see Figs. 3, *a* and *b*, and 4, *a* and *b*), these results suggest that the physically stronger intersubunit contact as well is along, and not between, the two long-pitch helical strands. In contrast, with phalloidin-stabilized F-actin filaments no significant local unraveling was observed.

Determination of Successive Crossover Spacings Along Individual Filament Stretches

Both in negatively stained (Hanson, 1967) and frozen-hydrated (Trinick et al., 1986; Stokes and DeRosier, 1987) F-actin filament preparations, the crossover spacings of the filaments appear to be intrinsically variable. Since the 3-D structures of unstabilized and phalloidin-stabilized F-actin filaments were significantly different (see above), we have quantitatively evaluated their respective crossover spacing frequency distributions. The procedure to measure succes-
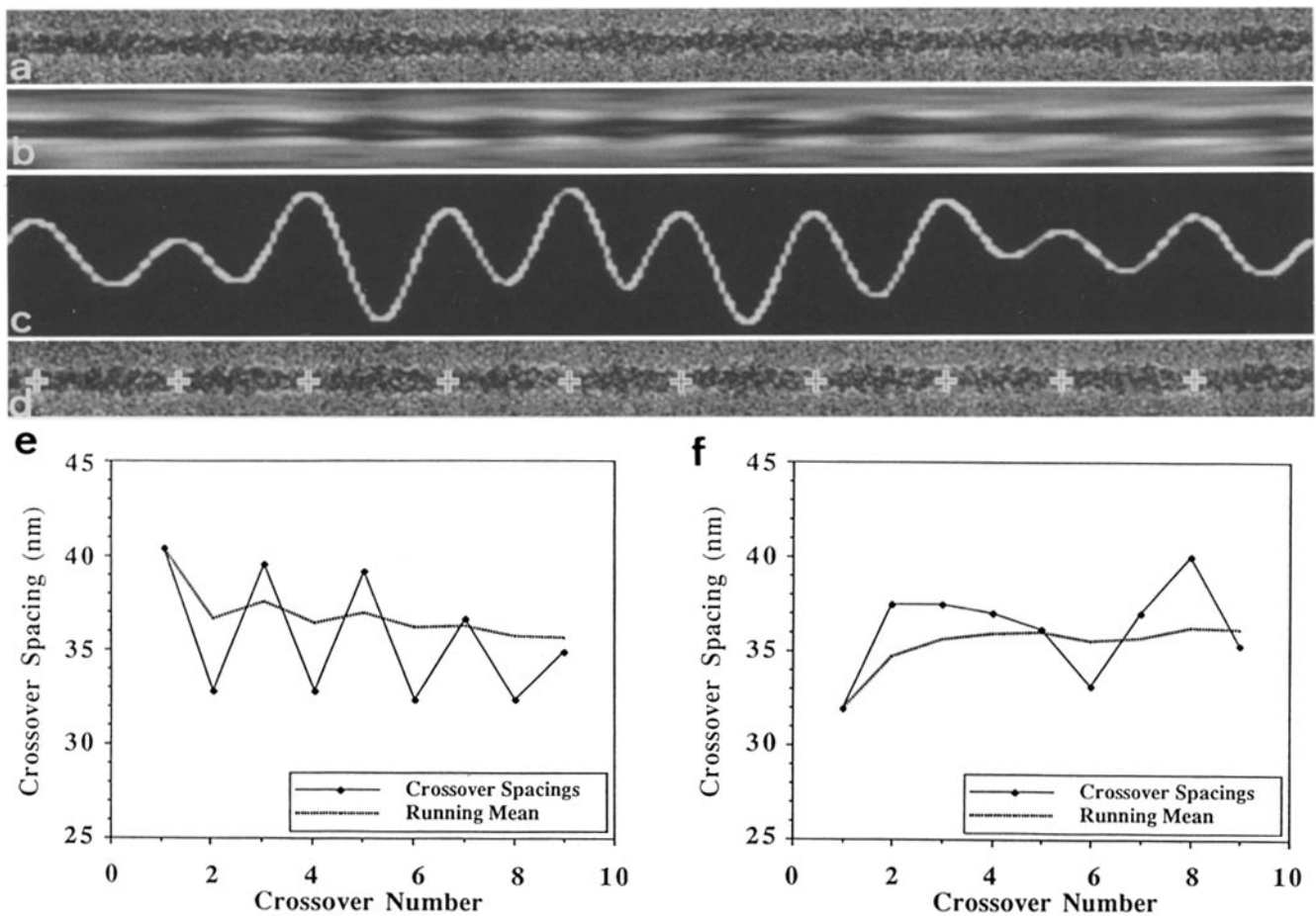
Figure 8. Quantitative evaluation of crossover spacings. An unbent nine-crossover long F-actin filament stretch (*a*) is Fourier-filtered (*b*) to mask out the spatial frequencies $\geq(30.0 \text{ nm})^{-1}$ and those $\leq(250.0 \text{ nm})^{-1}$. The filtered image is projected (i.e., by summing pixel values) perpendicular to the filament axis (*c*), a procedure revealing crossover points as local maxima. The filament stretch displayed in *a* with the crossover points as determined in *c* marked by crosses (*d*). The lower panels plot the crossover spacing versus the crossover number along nine-crossover long filament stretches. The filament stretch shown in *e* demonstrates compensatory deviations from the mean crossover spacing (i.e., long crossovers follow short ones and vice versa), while the filament stretch depicted in *f* contains a four-crossover stretch (i.e., defined by crossovers two to five) revealing relatively evenly spaced crossovers.

sive crossover spacings along a particular filament stretch is depicted in Fig. 8 (*a–d*): *a* displays an unbent 10-crossover long filament stretch; *b*, the same filament stretch with the spatial frequencies $\geq(30.0 \text{ nm})^{-1}$ and $\leq(250.0 \text{ nm})^{-1}$ masked out by Fourier-filtering; *c*, the projection (i.e., the sum of the pixel values) of *b* perpendicular to the filament axis; and *d*, the filament stretch from *a* with crosses superimposed to mark the crossovers corresponding to the peaks of the projection shown in *c*. In *e* and *f*, the successive crossover spacings of two nine-crossover long filament stretches are plotted. While the filament stretch in *e* reveals compensatory disorder (i.e., short crossovers follow long ones and vice versa), the stretch in *f* contains a four-crossover stretch (defined by crossovers two to five) with more or less evenly spaced crossovers. The latter type of filament stretches were used for 3-D helical reconstruction (see above).

As documented in Fig. 9 (*left panels*) for phalloidin-stabilized F-actin filaments the crossover spacing frequency distribution is significantly narrower (200 measurements; SD = 2.733 nm) than that of unstabilized F-actin filaments (200 measurements; SD = 3.359 nm), while the mean crossover spacings are virtually identical, i.e., 36.080 nm versus

36.085 nm. Consistent with this finding, in plots of average crossover spacing versus number of averaged crossovers, the "envelope" function (i.e., defined by overall mean $\pm$ 1 SD) appears narrower for phalloidin-stabilized F-actin filaments (Fig. 9, *lower right*) compared to that of unstabilized filaments (Fig. 9, *upper right*). As expected, in both cases, the overall mean does not significantly depend on the length of the filament stretches. This result suggests that the crossovers of phalloidin-stabilized F-actin filaments are more regularly spaced, i.e., less variable, than those of unstabilized F-actin filaments.

Discussion

The Backbone of the F-Actin Filament Is Formed by Two Long-Pitch Helical Strands of Uninterrupted High Mass Density

3-D helical reconstructions of negatively stained dispersed F-actin filaments reproducibly revealed two columns of uninterrupted mass density confined to filament radii ≤ 2.5 nm. The contact between neighboring subunits along these two
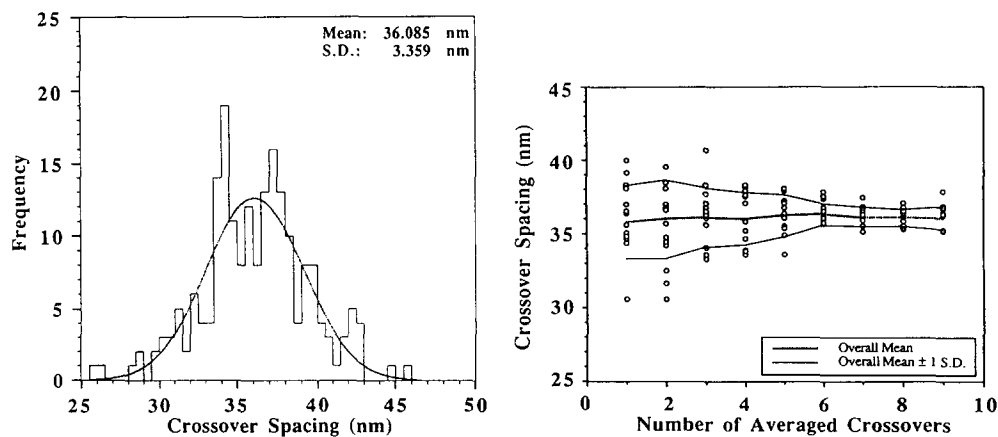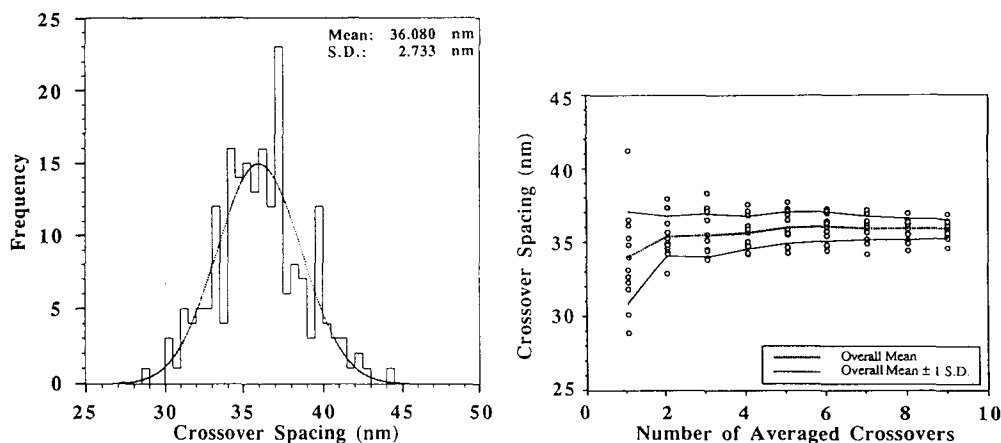
F-Actin Filaments

Figure 9. Comparison of the crossover spacing frequency distributions (*left panels*) and the running means along single filament stretches (*right panels*) for unstabilized F-actin filaments (*upper panels*) and phalloidin-stabilized F-actin filaments (*lower panels*). For the crossover spacing frequency distributions, 200 crossover values, each determined by the procedure outlined in Fig. 8, were included. Gaussian fits have been superimposed onto the histograms. For the running means, 13 9-crossover long filament stretches were analyzed for both unstabilized and phalloidin-stabilized filaments. Open circles represent the mean crossover spacing as a function of the number of crossovers averaged along the filament stretch (i.e., 1 to 9). The dotted line represents the overall mean (i.e., the average over all 13 values plotted) as a function of the number of crossovers averaged along the stretch, while the solid lines define an "envelope" function of overall mean ± 1 SD.

long-pitch helical strands (for nomenclature, see, e.g., Aebi et al., 1986) reproducibly persisted down to a contouring level to include 75% of the total mass and in many reconstructions down to 50%. By contrast, the contact between the two long-pitch helical strands always appeared to be of considerably lower mass density ranging from 100 to 75% mass, and it was more variable among reconstructions both in its mass density as well as in its spatial extent. A similar intersubunit bonding pattern has already been revealed in the first 3-D helical reconstruction of a negatively stained isolated thin filament (Moore et al., 1970) and later on from negatively stained dispersed F-actin filaments (Aebi et al., 1986), and it is a key feature of the atomic model of the actin filament (Holmes et al., 1990). By contrast, 3-D helical reconstructions of frozen-hydrated dispersed F-actin filaments (Trinick et al., 1986), and of S1-decorated thin and F-actin filaments (Milligan and Flicker, 1987) have revealed the major intersubunit contact between, and not along, the two long-pitch helices. The most recent 3-D reconstruction of frozen-hydrated F-actin filaments (Milligan et al., 1990) now too, yields significant intersubunit contact along the two long-pitch helical strands.

The average radius of gyration of all our F-actin filament reconstructions has been computed and found to be 2.58 ± 0.15 nm (mean ± SD), which is in excellent agreement with previously published values (Hartt and Mendelson, 1980; Smith et al., 1984; Egelman and Padron, 1984).

The Physically Stronger Intersubunit Contact within the F-Actin Filament Is Along, Not Between, the Two Long-Pitch Helical Strands

In all our negatively stained F-actin filament preparations, we frequently observed 2–6-subunit long filament stretches in which the genetic helix contact was completely broken thus yielding locally unraveled filament stretches (i.e., "loops" or "splayed ends"). Recently, such local unraveling has also been observed with negatively stained thin filaments (see Fig. 4 of Bennett and Marston, 1990) and with frozen-hydrated F-actin filaments (see Fig. 1 of Lepault et al., 1991). These observations can most easily be explained by assuming the physically stronger intersubunit contact being along rather than between the two long-pitch helical strands. In agreement with this argument, Erickson (1989) concluded from thermodynamic considerations that the bonds along the long-pitch helix should be approximately three times stronger than those along the genetic helix. Based on the atomic model of the F-actin filament (Holmes and Kabsch, 1991), this result seems plausible regarding the number of interacting residues, as well as the chemical nature of the interactions between them: almost exclusively mediated by hydrogen bonds and salt bridges, adjacent subunits make extensive, more or less stereospecific contact along the two long-pitch helical strands involving four binding sites of collectively 24 amino acid residues per subunit. In contrast, the weaker

though structurally important contact between the two long-pitch helical strands appears more floppy: it is mediated by hydrophobic interactions involving a six-residue binding site plus a four-residue loop inserted into a hydrophobic pocket formed by the interface of two adjacent subunits on the neighboring long-pitch helical strand.

The F-Actin Subunit Consists of an Inner and an Outer Domain and Is Distinctly Polar

The resolution of our F-actin filament reconstructions, extending to 2.5 nm axially and radially, has enabled us to reproducibly "cut out" the F-actin subunit which, if contoured to include 100% mass, measures 5.5 nm axially by ∼6.0 nm tangentially by ∼3.2 nm radially. As pictured in Fig. 5 d, distinct concavities on the inner and outer face of the F-actin subunit define a cleft separating the subunit into two domains of similar size, i.e., the inner domain I and the outer domain O. These two domains nicely correspond to the larger and smaller domain, respectively, of the atomic structure of the actin molecule (Kabsch et al., 1990). In both the atomic model of the actin filament (Holmes et al., 1990) as well as in our 3-D reconstructions of F-actin filaments, the larger domain is confined to low filament radii (i.e., ≤2.5 nm), forming the filament's "backbone" as two uninterrupted columns of high mass density defining the two long-pitch helical strands, while the smaller domain is placed at high filament radii (i.e., 2-5 nm). According to the nomenclature of Kabsch et al. (1990), the inner (I) or larger domain is composed of subdomains 3 and 4, while the outer (O) or smaller domain is composed of subdomains 1 and 2 (see Fig. 5 d).

Our F-actin subunit models are largely superimposable with the atomic structure when reduced to 2.5 nm resolution (Holmes and Kabsch, 1991). The small differences in the molecular dimensions of our subunit models and the atomic structure of the actin molecule, i.e., 5.5 × ∼6.0 × ∼3.2 nm versus 5.5 × 5.5 × 3.5 nm in Kabsch et al. (1990), may primarily be due to conformational changes occurring upon formation of the actin-DNase I complex, or upon polymerization into filaments (Harwell et al., 1980; Holmes et al., 1990; Kabsch et al., 1990). Obviously, some of the differences may also be attributed to specimen preparation artifacts due to surface tension phenomena and the use of negative stain. Therefore, it may be assumed that cryo-electron microscopy of frozen-hydrated material should minimize at least some of these possible artifacts. Surprisingly, however, the first 3-D reconstructions of frozen-hydrated F-actin filaments have yielded subunits which were too short to establish a long-pitch helix contact: while the axial subunit spacing amounts to 5.5 nm (Hanson and Lowy, 1967; reviewed in Aebi et al., 1986), the subunits revealed by Trinick et al. (1986) as well as Milligan and Flicker (1987) only measured 4 nm axially. In contrast, the recent 3-D reconstruction of frozen-hydrated F-actin filaments by Milligan et al. (1990) now resembles our 3-D reconstructions. However, comparison with the atomic structure reduced to a resolution of 2.5 nm reveals that the resolution of the "Milligan" model is somewhat lower than that of our model (compare, e.g., Figs. 3, a and b with Figs. 4, a and b of Holmes and Kabsch [1991]).

It has been argued that the actin structure determined from the actin-DNase I co-crystals may significantly deviate from the G- or F-actin conformation in those regions of the molecule that are in tight contact with DNase I, e.g., subdomain

2 or at least the "DNase I binding loop" forming its tip (Holmes et al., 1990; Holmes and Kabsch, 1991). To this end, F-actin filament reconstructions both from frozen-hydrated (Milligan et al., 1990), and to a lesser extent negatively stained (see Figs. 3 and 5) specimens yield relatively little mass in the area of subdomain 2, indicating that in the filament this subdomain is disordered, or deformed to overlap with subdomain 4. In fact, this low mass density in the area of subdomain 2 renders the F-actin subunit distinctly polar, consisting of a massive base and a slender tip in the direction of the filament axis (see Fig. 5; see also Milligan et al. [1990]). This intrinsic polarity prompted us to determine the orientation of our subunit models relative to the barbed and pointed filament ends as revealed by the arrowhead pattern of partially S1-decorated filaments. Accordingly, and consistent with the polarity deduced for the atomic filament model (Holmes et al., 1990), the massive base points towards the barbed end while the slender tip is oriented towards the pointed end of the filament. In agreement with earlier findings of Vibert and Craig (1982) and O'Brien et al. (1983), this subunit polarity gives rise to the distinct "mini-arrowhead" pattern depicted in helically filtered images of F-actin filaments whose polarity is opposite to that of the S1-decoration pattern (see Fig. 6).

Phalloidin Stabilizes F-Actin Filaments by Strengthening the Genetic Helix Contact

The bicyclic hepta-peptide toxin phalloidin, one of the toxins of the toadstool *Amanita phalloides* (Wieland and Faulstich, 1978), has been shown to stabilize F-actin filaments as judged (a) by a substantially decreased critical concentration for filament polymerization (reviewed in Cooper, 1987), and (b) by a very low background of monomers and small oligomers observed in our negatively stained F-actin filament preparations. Most importantly, this phalloidin-mediated stabilization resulted in a significantly smaller crossover spacing variation and, concomitantly, in a substantially reduced local unraveling of the filaments. Consistent with these findings, compared with our 3-D reconstructions of unstabilized F-actin filaments, those of phalloidin-stabilized filaments revealed a more massive "bridge" between the two long-pitch helical strands, thus, increasing the mass density of the intersubunit contact along the genetic helix.

Using affinity-labeling derivatives of phalloidin, Vandekerckhove et al. (1985) mapped the phalloidin binding site(s) of F-actin to include amino acid residues Glu_{117}, Met_{119}, and Met_{355}. According to the atomic model of the actin filament (Holmes et al., 1990), these three residues localize to the inner face (i.e., that facing the adjacent long-pitch helical strand) of subdomain 1 towards the bottom of the subunit. In fact, the thus defined phalloidin binding site forms part of the massive bridge connecting the two long-pitch helical strands. However, the mass of this bridge is far too large to be simply accounted for by a phalloidin molecule ($M_r = 789$ D) intercalated between the two strands, thus being indicative of some of the subunit distortions accompanying phalloidin binding to F-actin (Harwell et al., 1980; Wieland et al., 1975).

The Structural Basis for the Intrinsic Disorder of the Actin Filament: Lateral Slipping versus Random Twist

With its variable crossover spacings (Hanson, 1967) and fila-

ment width (reviewed by Aebi et al., 1986) that are independent of the method of preparation or measurement (Stokes and DeRosier, 1987), the F-actin filament appears to be an intrinsically disordered structure (Aebi et al., 1986; Trinick et al., 1986; Stokes and DeRosier, 1987; Lepault et al., 1991). To quantitate the variable crossover spacings, Egelman et al. (1982) have modeled the F-actin helix by a constant axial rise per subunit but a random variable twist between subunits. In this model the angular RMS (root-mean-square) deviation per subunit has been allowed to accumulate from one subunit to the next, thereby generating "cumulative angular disorder". Based on this model, Stokes and DeRosier (1987) have measured a mean rotational freedom between adjacent subunits along the genetic helix of ~12° for both negatively stained and frozen-hydrated F-actin filaments, and they have further shown that this torsional flexibility is modulated by actin-binding proteins. With the physically stronger inter-subunit contact being along, and not between, the two long-pitch helical strands (see above), such an amount of angular disorder would yield a displacement of ~0.6 nm between neighboring subunits within the long-pitch helical strands. While Egelman and DeRosier (1991) feel that a priori such type and amount of structural disorder does not conflict with the general principles of protein structure, it is difficult to reconcile with the known precision and rigidity of protein-protein interactions in general (reviewed in Erickson, 1989), and the intersubunit bonding pattern revealed in the atomic model of the actin filament in particular (Holmes et al., 1990; Holmes and Kabsch, 1991).

While in principle, a genetic helix with a random variable twist can model the generally observed variable crossover spacings of the actin filament in a simple and elegant way, it cannot account for variable filament width and local unraveling of the actin filament into its two long-pitch helical strands. Based on the observations reported in this paper, to a first approximation, the actin filament may behave as two rather independent strands of F-actin subunits, i.e., the two long-pitch helical strands, that may predominantly laterally slip past each other roughly perpendicular to the filament axis. While it is plausible that such "lateral slipping" gives rise to both variable crossovers and width of the actin filament, unlike random variable twist (for the formalism see Stokes and DeRosier, 1987), it cannot as easily be parametrized and hence, at this stage, only represents a qualitative description of the intrinsic disorder of the actin filament. One reason for this is that we do not yet know the exact mechanism underlying lateral slipping, i.e., how to decompose this movement into a radial and an angular component. An important feature of lateral slipping is that short-range it is "cumulative" while long-range it is "compensatory": it builds up over a few subunits and then reverses again, thus giving rise to longer and shorter crossovers, and hence to local under- and over-twisting of the two long-pitch helical strands.

Consistent with lateral slipping, in 3-D reconstructions of rigor insect flight muscle from tilted sections Taylor et al. (1984; 1989 a,b) have found both the separation and the twist of the two long-pitch helical strands, instead of being constant, to be locally perturbed in regions where crossbridges bound. Also, our analysis of successive crossover spacings (see Fig. 9) has revealed that, unless the variations are small, usually after one or at most two long crossovers follows a

short one and vice versa, such that already after two or three crossovers the running mean of the crossover spacing becomes very stable, just as predicted by compensatory lateral slipping of the two long-pitch helical strands. Last but not least, in extreme cases lateral slipping may result in complete separation of the two long-pitch helical strands over short (e.g., 2–6-subunit long) filament stretches, thus yielding locally unraveled filaments in the form of "loops" and "splayed ends" (see Fig. 7; and also Fig. 1 b of Lepault et al., 1991). Local unraveling, while readily explained by the lateral slipping model, cannot easily be explained in terms of a random twist model that assumes predominant genetic helix contact.

The wide range of published values for the actin filament width (i.e., 6–10 nm; see Aebi et al., 1986 and references therein) has generally been ascribed to variable amounts of spread-flattening of the filaments upon adsorption to the support film (e.g., Smith et al., 1984) or to uncertainties in measuring filament widths from stain exclusion patterns (e.g., Egelman and DeRosier, 1983). As an alternative, varying extents of lateral slipping may contribute significantly to this variability. Supporting this notion, ours as well as other published micrographs of negatively stained (e.g., Bullard et al., 1985; Aebi et al., 1986) as well as frozen-hydrated (e.g., Lepault et al., 1991) actin filaments often reveal substantial width variation along one and the same filament.

The intrinsic disorder of the F-actin filament appears to be governed predominantly by the physical strength of the intersubunit contacts between the two long-pitch helical strands, that in turn are modulated by the conformational state of the actin subunits. One such modulator is phalloidin which, according to our 3-D reconstructions, stabilizes the contacts between the two long-pitch helical strands. It may achieve this by inducing a conformational change of the actin subunit rather than acting as a "crosslinker" between the two strands (see above). Several pieces of experimental evidence suggest that depending on the state of hydrolysis of the bound nucleotide, both G- and F-actin will assume different conformations: (a) the critical concentration for ADP-G-actin to form F-actin filaments is 25–50-fold higher than that of ATP-G-actin (reviewed by Carlier et al., 1989); (b) Janmey et al. (1990) have found that ADP-F-actin filaments polymerized from ATP-G-actin are stiff rods, whereas ADP-F-actin filaments made from ADP-G-actin are flexible. Also, our own recent data have revealed local unraveling, and variation of the crossover spacing and filament width to depend on the state of hydrolysis of the bound nucleotide (Bremer, A., R. Sütterlin, A. Engel, and U. Aebi. 1990. J. Cell Biol. 111: 29a). Accordingly, these variations are minimal with ATP- or AMP-PNP-F-actin, intermediate with ADP-F-actin, and maximal with ADP-P$_i$-F-actin. As pronounced local unraveling of ADP-F-actin filaments is also observed after negative staining with Na-phosphotungstate (see Fig. 7 b), it is conceivable that Na-phosphotungstate may act as an inorganic phosphate analog similar to vanadate, BeF$_3^-$ or AlF$_4^-$ (Combeau and Carlier, 1988). Last, but not least, our preliminary results suggest that a "switch" in the intersubunit bonding pattern from predominant long-pitch helix to predominant genetic helix intersubunit contacts may occur depending on whether Ca^{2+} or Mg^{2+} is bound to the cation binding site(s) (Bremer, A., R. Sütterlin, A. Engel, and U. Aebi. 1990. J. Cell Biol. 111:29a).

Taken together, the intrinsic disorder of F-actin, the extent of which appears to be modulated by the state of hydrolysis of the bound nucleotide, may enable the actin moiety to play a more active role in actin-myosin-based force generation than merely act as a rigid passive cable as has hitherto been assumed.

References

Aebi, U., W. E. Fowler, T. D. Pollard, and P. R. Smith. 1981. Crystalline actin sheets: their structure and polymorphism. *J. Cell Biol.* 91:340–351.

Aebi, U., R. Millonig, H. Salvo, and A. Engel. 1986. The three-dimensional structure of the actin filament revisited. *Ann. N.Y. Acad. Sci.* 483:100–119.

Aebi, U., and T. D. Pollard. 1987. A glow discharge unit to render electron microscope grids and other surfaces hydrophilic. *J. Electr. Microsc. Tech.* 7:29–33.

Amos, L. A. 1985. The structure of muscle filaments studied by electron microscopy. *Annu. Rev. Biophys.* 14:291–313.

Bennett, P. M., and S. B. Marston. 1990. Calcium regulated thin filaments from molluscan catch muscle contain a caldesmon-like regulatory protein. *J. Muscle Res. Cell Motil.* 11:302–312.

Bullard, B., R. Bell, R. Craig, and K. Leonard. 1985. Arthrin: a new actin-like protein in insect flight muscle. *J. Mol. Biol.* 182:443–454.

Carlier, M.-F. 1989. Role of nucleotide hydrolysis in the dynamics of actin filaments and microtubules. *Int. Rev. Cytol.* 115:139–170.

Combeau, C., and M.-F. Carlier. 1988. Probing the mechanism of ATP hydrolysis on F-actin using vanadate and the structural analogs of phosphate BeF₃⁻ and AlF₄⁻. *J. Biol. Chem.* 263:17429–17436.

Cooper, J. A. 1987. Effects of cytochalasin and phalloidin on actin. *J. Cell Biol.* 105:1473–1478.

Cooper, J. A., and T. D. Pollard. 1982. Methods to measure actin polymerization. *Methods Enzymol.* 85:182–210.

DeRosier, D., and R. Censullo. 1981. Structure of F-actin needles from extracts of sea urchin oocytes. *J. Mol. Biol.* 146:77–99.

DeRosier, D., and P. B. Moore. 1970. Reconstruction of three-dimensional images from electron micrographs of structures with helical symmetry. *J. Mol. Biol.* 52:355–369.

Dierckx, P. 1980. An algorithm for cubic spline fitting with convexity constraints. *Computing.* 24:349–371.

Egelman, E. H. 1985. The structure of F-actin. *J. Muscle Res. Cell Motil.* 6:129–151.

Egelman, E. H. 1986. An algorithm for straightening images of curved filamentous structures. *Ultramicroscopy.* 19:367–374.

Egelman, E. H., and D. DeRosier. 1983. A model for F-actin derived from image analysis of isolated filaments (appendix). *J. Mol. Biol.* 166:623–629.

Egelman, E. H., and D. J. DeRosier. 1991. Angular disorder in actin: is it consistent with general principles of protein structure? *J. Mol. Biol.* 217:405–408.

Egelman, E. H., and R. Padron. 1984. X-ray evidence that actin is a 100 Å filament. *Nature (Lond.).* 307:56–58.

Egelman, E. H., N. Francis, and D. DeRosier. 1982. F-actin is a helix with a random variable twist. *Nature (Lond.).* 298:131–135.

Erickson, H. P. 1989. Co-operativity in protein-protein association: the structure and stability of the actin filament. *J. Mol. Biol.* 206:465–474.

Faulstich, H., H. J. Schäfer, and M. Weckauf. 1977. The dissociation of the phalloidin-actin complex. *Hoppe-Seyler's Z. Physiol. Chem.* 10:181–186.

Flaherty, K. M., D. B. McKay, W. Kabsch, and K. C. Holmes. 1991. Similarity of the three-dimensional structures of actin and the ATPase fragment of a 70-KDa heat shock cognate protein. *Proc. Natl. Acad. Sci. USA.* 88:5041–5045.

Hanson, J. 1967. Axial period of actin filaments. *Nature (Lond.).* 213:353–356.

Hanson, J., and J. Lowy. 1963. The structure of F-actin and of actin filaments isolated from muscle. *J. Mol. Biol.* 6:46–60.

Hartt, J., and R. Mendelson. 1980. X-ray scattering of F-actin and myosin subfragment-1 complex. *Fed. Proc.* 39:1729.

Harwell, D. O., M. L. Sweeney, and F. H. Kirkpatrick. 1980. Conformation changes of actin during formation of filaments and paracrystals and upon interaction with DNase I, cytochalasin B, and phalloidin. *J. Biol. Chem.* 255:1210–1220.

Holmes, K. C., and W. Kabsch. 1991. Muscle proteins: actin. *Curr. Opin. Struct. Biol.* 1:270–280.

Holmes, K. C., D. Popp, W. Gebhard, and W. Kabsch. 1990. Atomic model of the actin filament. *Nature (Lond.).* 347: 44–49.

Huxley, H. E. 1963. The structure of F-actin and of actin filaments isolated from muscle. *J. Mol. Biol.* 7:281–308.

Janmey, P. A., S. Hvidt, G. F. Oster, J. Lamb, T. P. Stossel, and J. H. Hartwig. 1990. Effect of ATP on actin filament stiffness. *Nature (Lond.).* 347:95–99.

Kabsch, W., H. G. Mannherz, and D. Suck. 1985. Three-dimensional structure of the complex of actin and DNAse I at 4.5 Å resolution. *EMBO (Eur. Mol. Biol. Organ.) J.* 4:2113–2118.

Kabsch, W., H. G. Mannherz, D. Suck, E. Pai, and K. C. Holmes. 1990. Atomic structure of the actin:DNase I complex. *Nature (Lond.).* 347:37–44.

Lepault, J., I. Erk, G. Nicolas, and J.-L. Ranck. 1991. Time-resolved cryoelectron microscopy of vitrified muscular components. *J. Microsc.* 161: 47–57.

Lorensen, W. E., and H. E. Cline. 1987. Marching cubes: a high resolution surface construction algorithm. *Computer Graphics.* 21:163–169.

Milligan, R. A., and P. F. Flicker. 1987. Structural relationships of actin, myosin, and tropomyosin revealed by cryo-electron microscopy. *J. Cell Biol.* 105:29–39.

Milligan, R. A., M. Whittaker, and D. Safer. 1990. Molecular structure of F-actin and location of surface binding sites. *Nature (Lond.).* 348:217–221.

Millonig, R. C., H. Salvo, and U. Aebi. 1988. Probing actin polymerization by intermolecular cross-linking. *J. Cell Biol.* 106:785–796.

Moore, P. B., H. E. Huxley, and D. J. DeRosier. 1970. Three-dimensional reconstruction of F-actin, thin filaments and decorated thin filaments. *J. Mol. Biol.* 50:279–295.

O'Brien, E. J., J. Couch, G. R. P. Johnson, and E. P. Morris. 1983. Structure of actin and the thin filament. *In* Actin: Its Structure and Function in Muscle and Non-Muscle Cells. C. DosRemedios and J. Barden, editors. Academic Press, Sydney, Australia. 3–15.

Pollard, T. D. 1990. Actin. *Curr. Opin. Cell Biol.* 2:33–40.

Sakabe, N., K. Sakabe, K. Sasaki, H. Kondo, T. Ema, N. Kamiya, and M. Matsushima. 1983. Crystallographic studies on the chicken gizzard G-actin·DNase I complex at 5 Å resolution. *J. Biochem. (Tokyo).* 93:299–302.

Saxton, O. W., T. J. Pitt, and M. Horner. 1979. Digital image processing: the semper system. *Ultramicroscopy.* 4:343–354.

Schutt, C. E., U. Lindberg, J. Myslik, and N. Strauss. 1989. Molecular packaging in profilin: actin crystals and its implications. *J. Mol. Biol.* 209: 735–746.

Seymour, J., and E. J. O'Brien. 1980. The position of tropomyosin in muscle thin filaments. *Nature (Lond.).* 283:680–682.

Smith, P. R. 1978. An integrated set of computer programs for processing electron micrographs of biological structures. *Ultramicroscopy.* 3:153–160.

Smith, P. R., and U. Aebi. 1974. Computer generated Fourier transforms of helical particles. *J. Phys. A: Gen. Phys.* 7:1627–1633.

Smith, P. R., U. Aebi, R. Josephs, and M. Kessel. 1976. Studies on the structure of the bacteriophage T4 tail sheath. I. The recovery of 3-D structural information from the extended sheath. *J. Mol. Biol.* 106:243–271.

Smith, P. R., W. E. Fowler, and U. Aebi. 1984. Toward an alignment of the actin molecule in the actin filament. *Ultramicroscopy.* 13:113–124.

Smith, P. R., W. E. Fowler, T. D. Pollard, and U. Aebi. 1983. Structure of the actin molecule determined from electron micrographs of crystalline actin sheets with a tentative alignment of the molecule in the actin filament. *J. Mol. Biol.* 167:641–660.

Steven, A. C., R. Stall, P. M. Steinert, and L. T. Benes. 1985. Computational straightening of images of filamentous helices by cubic spline interpolation facilitates structural analysis by Fourier methods. *In* Proceedings of the 43rd Annual Meeting of the Electron Microscopic Society of America. G. W. Bailey, editor. 738–739.

Stokes, D. L., and DeRosier, D. L. 1987. The variable twist of actin and its modulation by actin-binding proteins. *J. Cell Biol.* 104:1005–1017.

Taylor, K. A., and L. A. Amos. 1981. A new model for the geometry of the binding of myosin crossbridges to muscle thin filaments. *J. Mol. Biol.* 147:297–324.

Taylor, K. A., M. C. Reedy, L. Cordova, and M. Reedy. 1984. Three-dimensional reconstruction of rigor insect flight muscle from tilted thin sections. *Nature (Lond.).* 310:285–291.

Taylor, K. A., M. C. Reedy, L. Córdova, and M. K. Reedy. 1989a. Three-dimensional image reconstruction of insect flight muscle. I. The rigor myac layer. *J. Cell Biol.* 109:1085–1102.

Taylor, K. A., M. C. Reedy, L. Córdova, and M. K. Reedy. 1989b. Three-dimensional image reconstruction of insect flight muscle. I. The rigor actin layer. *J. Cell Biol.* 109:1103–1123.

Trinick, J., J. Cooper, J. Seymour, and E. H. Egelman. 1986. Cryo-electron microscopy and three-dimensional reconstruction of actin filaments. *J. Microsc.* 141:349–360.

Vandekerckhove, J. 1990. Actin-binding proteins. *Curr. Opin. Cell Biol.* 2:41–50.

Vandekerckhove, J., A. Deboben, M. Nassai, and T. Wieland. 1985. The phalloidin binding site of F-actin. *EMBO (Eur. Mol. Biol. Organ.) J.* 4:2815–

2818.

Vibert, P., and R. Craig. 1982. Three-dimensional reconstruction of thin filaments decorated with a Ca^{2+}-regulated myosin. *J. Mol. Biol.* 157:299–319.

Wieland, T., and H. Faulstich. 1978. Amatoxins, phallotoxins, phallolysin, and antamanide: the biologically active components of poisonous *Amanita* mushrooms. *CRC Crit. Rev. Biochem.* 5:185–260.

Wieland, T., X. de Vries, A. Schäfer, and H. Faulstich. 1975. Spectroscopic evidence for the interaction of phalloidin with actin. *FEBS (Fed. Eur. Biochem. Soc.) Lett.* 54:73–75.

Wrigley, N. G. 1968. The lattice spacing of crystalline catalase as an internal standard of length in electron microscopy. *J. Ultrastruct. Res.* 24:454–464.